X-ray Study of the Spinel $LiMn_2O_4$ at Low Temperatures

G. Rousse and C. Masquelier*

Laboratoire de Chimie des Solides, Université Paris-Sud, 91405 Orsay Cedex, France

J. Rodríguez-Carvajal

Laboratoire Léon Brillouin (CEA-CNRS), CEA/Saclay, 91191 Gif sur Yvette Cedex, France

E. Elkaim and J.-P. Lauriat

LURE, Université Paris-Sud, 91405 Orsay Cedex, France

J. L. Martínez

Instituto de Ciencia de Materiales de Madrid, CSIC, Cantoblanco, Madrid E-28049, Spain

Received July 7, 1999. Revised Manuscript Received September 30, 1999

Stoichiometric $LiMn_2O_4$ undergoes a structural phase transition close to room temperature from cubic to orthorhombic symmetry. The crystal structure at 230 K (space group *Fddd* and $a = 24.743(1)$, $b = 24.840(1)$, and $c = 8.199(1)$ Å) corresponds to an orthorhombic $\sim 3a \times 3a \times a$ superstructure of the cubic spinel structure, induced by a charge ordering on the manganese sites. By use of synchrotron X-ray diffraction, it is shown that the transition is first-order with the coexistence of two phases in a small range of temperatures and that the cell volume very slightly increases on cooling. Synchrotron X-ray diffraction confirms the symmetry of the low-temperature phase and reveals that the orthorhombic phase studied at 230 K progressively shifts to a symmetry close to tetragonal when cooled to lower temperatures. However, the symmetry of $LiMn_2O_4$ is never tetragonal, even down to 1.5 K, and this tends to exclude the onset to a complete charge-ordered state.

Introduction

Compositions belonging to the solid solution $Li[Li_xMn_{2-x}]O_4$ are potential candidates to be used as cathodes in Li-ion batteries,[1] provided the problems associated with capacity fading can be solved.[2] Recently, much attention has been paid to the physical properties of the spinel $LiMn_2O_4$, investigated by various techniques such as ^{6}Li and ^{7}Li NMR,[3,4] EXAFS and XANES spectroscopy,[5,6] infrared spectroscopy,[7] and diffraction techniques.[8] The phase transition around room temperature observed in stoichiometric $LiMn_2O_4$ is a matter of intense research, as it is believed to be partly at the origin of capacity fading problems when $LiMn_2O_4$ is used as the positive electrode in Li-ion cells. Recently, we have characterized this transition by neutron diffraction.[9] The resolution of the structure at 230 K indicated that a partial charge ordering on the Mn ions is established at $T < 290$ K. Contrary to what was observed in the Mn perovskites close to the composition $(R_{1/2}D_{1/2})MnO_3$ (R, trivalent rare earth; D, divalent ion), the charge ordering in $LiMn_2O_4$ can be univocally described because the superstructure reflections induced are very intense in neutron diffraction as in X-ray diffraction. The behavior of $LiMn_2O_4$ at lower temperatures was only scarcely mentioned; the onset of a totally ordered state was suggested,[9] and the onset of a new phase transition to tetragonal symmetry was reported.[10] This work intends to further clarify the nature of the cubic → orthorhombic transition around room temperature. The behavior of the orthorhombic form down to lower temperatures (10 K) is also presented.

Experimental Section

Stoichiometric $LiMn_2O_4$ was prepared as described elsewhere[11] and was characterized by X-ray and neutron diffraction techniques. X-ray diffraction was performed using synchrotron radiation on the WD4C wiggler beamline of the DCI ring of LURE (Orsay). To minimize absorption while keeping

* To whom correspondence should be addressed.

(1) Thackeray, M. M. *Prog. Solid St. Chem.* **1997**, *25*, 1 and references therein.
(2) Amatucci, G. G.; Schmutz, C. N.; Blyr, A.; Sigala, C.; Gozdz, A. S.; Larcher, D.; Tarascon, J. M *J. Power Sources* **1997**, *69*, 11.
(3) Lee, Y. J.; Wang, F.; Grey, C. P. *J. Am. Chem. Soc.* **1998**, *120*, 12601.
(4) Gee, B.; Horne, C. H.; Cairns, E. J.; Reimer, J. A. *J. Phys. Chem. B* **1998**, *102*, 10142.
(5) Ammundsen, B.; Jones, D. J.; Roziere J. *J. Solid State Chem.* **1998**, *141*, 294.
(6) Yamaguchi, H.; Yamada, A.; Uwe, H. *Phys. Rev.* **1998**, *B58*, 8.
(7) Paolone, A.; Roy, P.; Rousse, G.; Masquelier, C.; Rodriguez-Carvajal, *J. Solid State Commun.* **1999**, *111*, 453.
(8) Oikawa, K.; Kamiyama, T.; Izumi, F.; Chakoumakos, B.; Ituka, H.; Wakihara, M.; Li, J.; Matsui, Y. *Solid State Ionics* **1998**, *109* (1−2), 35.
(9) Rodríguez-Carvajal, J.; Rousse, G.; Masquelier, C.; Hervieu, M. *Phys. Rev. Lett.* **1998**, *81*, 4660.
(10) Hayakawa, H.; Takada, T.; Enoki, E.; Akiba, E. *J. Mater. Sci. Lett.* **1998**, *17*, 811.
(11) Rousse, G.; Masquelier, C.; Rodriguez-Carvajal, J.; Hervieu, M.; *Electrochem. Solid State Lett.* **1999**, *2* (1), 6.

10.1021/cm9910963 CCC: $18.00
Published on Web 11/19/1999

good resolution and flux, a wavelength of 1.073 Å was selected. Temperature-controlled measurements from 70−295 K were performed with a closed cycle cryostat (Displex APD Cryogenics) with the sample on an aluminum holder (reflection geometry).

For the measurements around room temperature, a small nitrogen blower (Oxford Cryosystems) was used to vary the temperature by steps of 1 K. These measurements were done in Debye−Scherrer geometry with the powder in a Lindemann capillary ($\varnothing = 300\ \mu$m). Patterns were collected after equilibrium of the sample for 30 min at a given temperature.

Additionally, X-ray diffraction was performed from 300 to 10 K, on a rotating-anode diffractometer apparatus equipped with a copper anticathode ($\lambda = 1.5418$ Å) and a graphite back-monochromator.

The program Fullprof[12] was used for crystal structure refinements using the Rietveld method.[13]

Specific heat measurements were performed between 2 and 350 K by the heat pulse relaxation method, under external applied magnetic fields up to 9 T in a physical properties measurement system (PPMS, from Quantum Design, San Diego). The measurement is adiabatic with a temperature stability better than 0.2%, and the temperature rise of the heat pulse was 2% of the base temperature. The measurements were performed on cooling and heating under different magnetic fields.

Results and Discussion

I. Charge Ordering of Manganese Ions (Neutrons). The good quality of our stoichiometric $LiMn_2O_4$ sample was controlled by X-ray and neutron diffraction.[9,11] The high-temperature form (cubic) was carefully studied by neutron diffraction at 350 K to confirm the crystalline quality and the stoichiometry of the sample. The refined structural parameters were the lattice parameter a, the oxygen parameter x of the Wyckoff site *32e* (space group $Fd\bar{3}m$, origin choice at inversion center), the occupation of the oxygen site, the isotropic temperature factor of Li, and the anisotropic temperature factors of Mn and O. The final Bragg R-factor was 1.2%. We obtained a lattice parameter $a = 8.249(1)$ Å (at 350 K) consistent with other publications concerning stoichiometric samples. The unique Mn−O distance is 1.961(1) Å, which is intermediate between what is expected for Mn^{3+}−O and Mn^{4+}−O bond lengths.[14]

It is now well-known that the stoichiometric $LiMn_2O_4$ undergoes a phase transition close to room temperature, which gives a beautiful signature in DSC.[11,15] The transition also induces a large modification of the conduction properties of the spinel: the conductivity decreases by 1 order of magnitude when the temperature is decreased below 290 K.[11,16] This transition is also associated with a change in entropy, as revealed by the great changes in the specific heat around room temperature (Figure 1). In the heating process, the entropy associated with the first-order phase transition is 17.85 J/K/mol. By contrast, on cooling, the change in entropy, as observed by the area of the specific heat curve, is 14.26 J/K/mol. The applied magnetic field has no influence on the phase transition; as expected for a structural phase transition, only the cooling or heating approaching to the first-order charge-ordering transition produces a remarkable effect on the specific heat peak. We recently solved the structure of $LiMn_2O_4$ at 230 K, by neutron diffraction, and we demonstrated the existence of a partial charge-ordered state[9] at low temperatures. The refinement of the pattern was made using an orthorhombic $\sim 3a \times 3a \times a$ super-cell, in the space group *Fddd*. This leads to a big unit cell with five manganese, four lithium, and nine oxygen in the asymmetric unit.

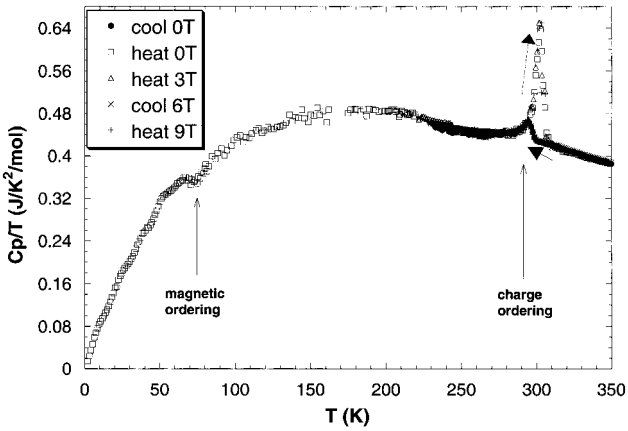

Figure 1. Specific heat of $LiMn_2O_4$, on heating (heat) and on cooling (cool) under different magnetic fields.

Table 1 presents the oxygen octahedral environment for each of the five manganese sites; Mn−O distances and O−Mn−O angles are reported, as well as the average Mn−O distance and the distortion of the octahedron, given by the following formula: $\Delta = (1/N)\Sigma_{n=1,N}\{(d_n - \langle d\rangle)/\langle d\rangle\}^2$. The valence bond sum is calculated using the Zachariasen formula: $V_i = \Sigma_j s_{ij} = \Sigma \exp\{(d_0 - d_{ij})/0.37\}$ using the parameter d_0, characterizing a cation−anion pair. These calculations have been performed assuming a d_0 of Mn^{3+}−O^{2-} for Mn(1)−Mn(3) and a d_0 of Mn^{4+}−O^{2-} for Mn(4) and Mn(5). The Mn(1)O_6 octahedron (Mn on the special position 16d) is distorted: it is elongated along [001] and compressed along [010]. However, the O−Mn−O angles are not very different from the angles expected for a regular octahedron. The average Mn−O distance of 2.00 Å indicates that this Mn is close to trivalent. The local distortion of this octahedron is also in good agreement with the Jahn−Teller effect of the Mn^{3+}. The Mn(2)O_6 octahedron is elongated along [100] and compressed along [010]. The Mn(3)O_6 octahedron is also found to be nearly trivalent, with an elongation along [010] and a compression along [001]. From these considerations, it follows that the three Mn^{3+}-type ions are elongated along the three different main crystallographic directions, so that the cell distortion remains very short. The Mn(4) and Mn(5) ions do not present such differences in their Mn−O distances and O−Mn−O angles. They are purely Mn^{4+} ions, for which the distortion is much smaller. These ions are not located in the center of the octahedra: for Mn(5), the longest (1.97 Å) and the shortest (1.83 Å) Mn−O lengths are directed along [100].

The Mn^{3+} are distributed in a columnar fashion along [001] and are surrounded by Mn^{4+} ions. This peculiar

(12) Rodriguez-Carvajal, J. *Physica B* **1993**, *192*, 55. See http://www-llb.cea.fr/fullweb/powder.htm.
(13) Rietveld, H. M. *J. Appl. Crystallogr.* **1969**, *2*, 65.
(14) Brown, I. D.; Altermatt, D. *Acta Crystallogr.* **1985**, *B41*, 244.
(15) Yamada, A.; Tanaka, M. *Mater. Res. Bull.* **1995**, *30*, 715.
(16) Shimakawa, Y.; Numata, T.; Tabuchi, J. *J. Solid State Chem.* **1997**, *131*, 138.

Table 1. Mn−O Distances (Å, diagonal) and O−Mn−O Angles (deg) in MnO_6 Octahedra for Each Mn Site[a]

Mn(1)	O(2)ii	O(2)vi	O(4)i	O(4)v	O(5)ii	O(5)vi
O(2)ii	*1.9610 (54)*					av distance: 2.003(2)
O(2)vi	180.0 (5)	*1.9610 (54)*				distortion: 20.5×10^{-4}
O(4)i	86.5 (4)	93.4 (4)	*1.9194 (47)*			sums: 3.20(2)
O(4)v	93.4 (4)	86.5 (4)	180.0 (5)	*1.9194 (47)*		
O(5)ii	81.2 (4)	98.8 (4)	78.6 (3)	101.3 (4)	*2.1291 (46)*	
O(5)vi	98.8 (4)	81.2 (4)	101.3 (4)	78.6 (3)	180.0 (4)	*2.1291 (46)*

Mn(2)	O(1)ii	O(2)i	O(4)ii	O(9)i	O(9)ii	O(9)iv
O(1)ii	*2.0305 (86)*					av distance: 1.996(4)
O(2)i	81.9 (4)	*1.9571 (88)*				distortion: 18.7×10^{-4}
O(4)ii	79.4 (5)	82.4 (5)	*2.0796 (100)*			sums: 3.26(3)
O(9)i	95.5 (5)	176.6 (5)	99.3 (5)	*1.8835 (89)*		
O(9)ii	96.5 (5)	93.8 (5)	174.7 (6)	84.3 (5)	*2.1170 (103)*	
O(9)iv	179.1 (5)	98.3 (5)	99.8 (5)	84.3 (5)	84.3 (5)	*1.9079 (88)*

Mn(3)	O(3)i	O(3)iv	O(6)vi	O(7)i	O(7)iii	O(8)i
O(3)i	*1.9042 (139)*					av distance: 2.020(5)
O(3)iv	84.1 (6)	*2.2146 (94)*				distortion: 36.1×10^{-4}
O(6)vi	82.4 (6)	80.0 (5)	*1.9364 (106)*			sums: 3.12(4)
O(7)i	96.2 (6)	99.1 (5)	178.4 (6)	*1.9538 (112)*		
O(7)iii	175.2 (8)	100.6 (6)	97.4 (6)	84.0 (6)	*1.9481 (143)*	
O(8)i	93.8 (6)	177.4 (5)	101.2 (5)	79.6 (5)	81.5 (6)	*2.1634 (91)*

Mn(4)	O(1)i	O(3)vii	O(4)i	O(5)ii	O(6)i	O(6)iv
O(1)i	*1.9182 (91)*					av distance: 1.903(4)
O(3)vii	176.3 (6)	*1.8735 (95)*				distortion: 5.4×10^{-4}
O(4)i	88.3 (6)	95.0 (6)	*1.8511 (120)*			sums: 4.03(5)
O(5)ii	83.4 (5)	95.3 (5)	87.7 (6)	*1.8601 (96)*		
O(6)i	92.6 (5)	88.4 (5)	97.2 (6)	173.6 (6)	*1.9640 (95)*	
O(6)iv	93.9 (6)	82.8 (6)	177.8 (8)	92.9 (6)	82.3 (6)	*1.9515 (123)*

Mn(5)	O(1)i	O(2)ii	O(5)ii	O(7)i	O(8)i	O(8)iii
O(1)i	*1.9219 (78)*					av distance: 1.915(4)
O(2)ii	84.9 (5)	*1.9516 (104)*				distortion: 5.8×10^{-4}
O(5)ii	80.3 (4)	85.5 (5)	*1.9729 (92)*			sums: 3.90(4)
O(7)i	173.9 (5)	92.5 (5)	93.9 (5)	*1.9347 (74)*		
O(8)i	96.9 (5)	96.6 (6)	176.4 (6)	88.9 (5)	*1.8353 (92)*	
O(8)iii	92.9 (5)	177.8 (7)	94.0 (5)	89.7 (5)	83.8 (5)	*1.8772 (105)*

[a] i: x, y, z. ii: $-x + 3/4, -y + 3/4, z$. iii: $-x + 3/4, y, -z + 3/4$. iv: $x, -y + 3/4, -z + 3/4$. v: $-x, -y, -z$. vi: $x + 1/4, y + 1/4, -z$. vii: $x + 1/4, -y, z + 1/4$. viii: $-x, y + 1/4, z + 1/4$.

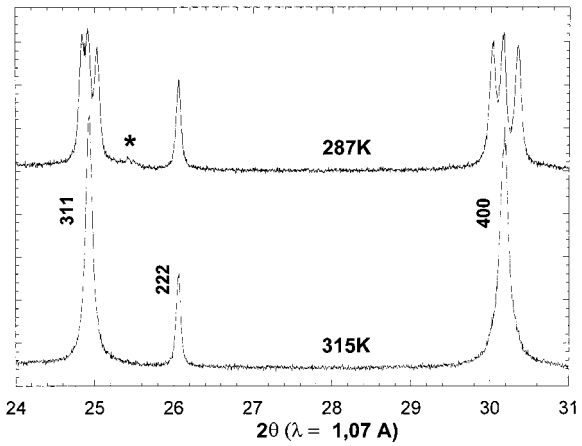

Figure 2. Part of the synchrotron X-ray diffraction patterns at 315 (cubic phase) and 287 K (orthorhombic phase). Indices refer to the cubic phase. Note the splitting of the (311) and (400) reflections, compared to the (222) reflection. The star indicates the most intense superlattice reflection.

charge ordering gives a clue for understanding the conductivity behavior.[9,16]

II. Synchrotron X-ray Diffraction Study of the Transition. Around room temperature, synchrotron radiation allowed us to carefully study the mechanism of the transition.

Figure 2 presents parts of the patterns recorded at 287 K (purely orthorhombic phase) and at 315 K (purely cubic) on heating. From a cubic structure with a lattice parameter a, decreasing the temperature induces an orthorhombic structure with the following lattice parameters: $a(1 + \epsilon_1)$, $a(1 + \epsilon_2)$, $a(1 + \epsilon_3)$, if one considers the orthorhombic distortion of the cell only. For a complete indexing of the charge ordering superstructure reflections in the diffraction pattern, the a and b parameters have to be tripled.

For an (hkl) reflection in the orthorhombic average cell,

$$\frac{1}{d_{hkl}{}^2\text{ortho}} = \frac{h^2}{a^2(1+\epsilon_1)^2} + \frac{k^2}{a^2(1+\epsilon_2)^2} + \frac{l^2}{a^2(1+\epsilon_3)^2} \quad (1)$$

It follows from a first-order development that

$$\frac{1}{d_{hkl}{}^2\text{ortho}} = \frac{1}{d_{hkl}{}^2\text{cub}} - \frac{2}{a^2}(h^2\epsilon_1 + k^2\epsilon_2 + l^2\epsilon_3) \quad (2)$$

The (400) cubic reflection splits into three reflections:

$$\frac{1}{d_{400}{}^2\text{ortho}} = \frac{1}{d_{400}{}^2\text{cub}} - \frac{32}{a^2}\epsilon_1 \quad (3)$$

$$\frac{1}{d_{040}{}^2\text{ortho}} = \frac{1}{d_{400}{}^2\text{cub}} - \frac{32}{a^2}\epsilon_2 \quad (4)$$

$$\frac{1}{d_{004}{}^2\text{ortho}} = \frac{1}{d_{400}{}^2\text{cub}} - \frac{32}{a^2}\epsilon_3 \quad (5)$$

The (222) cubic reflection remains a single peak with

$$\frac{1}{d_{222}{}^2\text{ortho}} = \frac{1}{d_{222}{}^2\text{cub}} - \frac{8}{a^2}(\epsilon_1 + \epsilon_2 + \epsilon_3) \quad (6)$$

The (311) cubic reflection splits into three reflections in the same way as the (400) reflection does. Within this 1st-order approximation, we can characterize the transition. Analysis of the evolution of the (400) and the (311) cubic reflections when decreasing the temperature gave access to $\epsilon_1 = 6 \times 10^{-4}$, $\epsilon_2 = 5.1 \times 10^{-3}$, and $\epsilon_3 = -5.5 \times 10^{-3}$.

The position of the (222) cubic reflection upon cooling does not change. No shift was observed. This means, from eq 6, that $\epsilon_1 + \epsilon_2 + \epsilon_3 = 0$, within experimental error, which is verified experimentally from the values given above and consequently, that the volume change at the transition is very small because, at first order, $V_{\text{ortho}} = V_{\text{cub}}(1 + \epsilon_1 + \epsilon_2 + \epsilon_3)$.

From the Rietveld refinement of the synchrotron data, we find $a = 8.2481(1)$ Å ($V = 561.13(1)$ Å^3) for the cubic phase at 326 K and $a = 24.7598(4)$, $b = 24.8710(4)$, and $c = 8.2028(1)$ Å for the orthorhombic phase at 305 K. The "average-cell" distortion is found to be $a = 8.253$, $b = 8.290$, and $c = 8.203(1)$ Å ($V = 561.25(1)$ Å^3). Note that the Rietveld refinement allows a precise determination of the cell parameters and hence to the cell volume. The later is not unchanged at the transition, as a slight increase is observed on cooling, as usually observed in charge-ordering transitions.

The evolution of the X-ray diffraction pattern with temperature was recorded by steps of 1 K, first on heating from the orthorhombic phase to the cubic phase and then on cooling to a complete transformation toward the orthorhombic phase. Part of this pattern that corresponds to the 2θ region of the (400) cubic reflection is plotted in Figure 3, between 288 (orthorhombic) and 315 K (cubic), on heating. Between 288 and 298 K, there is only a very minor shift in 2θ due to thermal expansion. From 298 K, and up to 311 K, the pattern evolves gradually as a quadruplet, due to the mixture of cubic and orthorhombic phases. Each pattern was fitted with a least-squares refinement, assuming that a pattern recorded at a temperature T can be described as the sum of two patterns: Pattern(T) = α. Pattern(pure cubic) + (1 − α). Pattern(pure orthorhombic), ($0 \le \alpha \le 1$), where α denotes the percentage of the cubic phase in the mixture. The good agreement between the observed pattern and the pattern deduced from this sum indicates that only the proportion between the two phases is changing with temperature. In particular, the lattice parameters of the cubic and of the orthorhombic phases remain unchanged during the transition. Note that the apparent shift in the maximum central peak is not the signature of the modification of the cubic phase during the transition. This shift is only due to the evolution of the ratio between the cubic and orthorhombic phases, as ϵ_1 is not equal to zero. Figure 4 presents the ratio α of the cubic phase, on cooling and on heating. One can first note the existence of a small hysteresis of a few Kelvin. On cooling, the orthorhombic phase begins to appear at 295 K, and on heating, the cubic phase appears at 298 K. There then follows a domain with the coexistence of the two phases, characteristic of a first-order transition. This is consistent with the DSC measurements around room temperature at different heating and cooling rates (Figure 5). At a high heating and cooling rate (e.g., 20 K/min) the hysteresis is of approximately 30 K. When decreasing the rates to 0.5 K/min, the hysteresis is only of 5 K. Here, the synchrotron data correspond to a measure of the transition with an extremely small rate, as the sample was allowed to equilibrate at a given temperature for 30 min before each scan. Note that the enthalpy of the transition is independent of the heating and cooling rates. Its value is 1.75 kJ/mol.

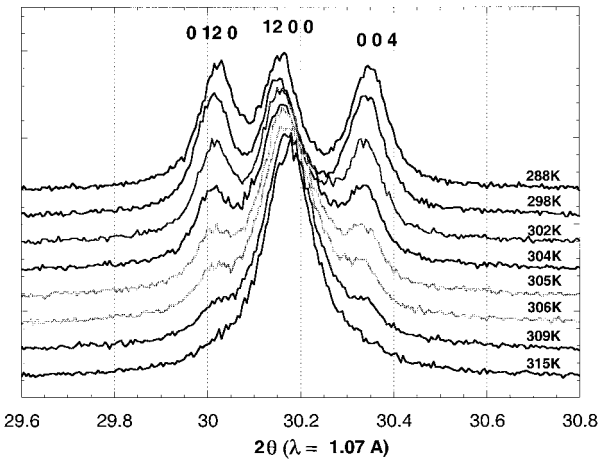

Figure 3. Evolution of the (400) cubic reflection during the transition, on heating from 288 to 315 K.

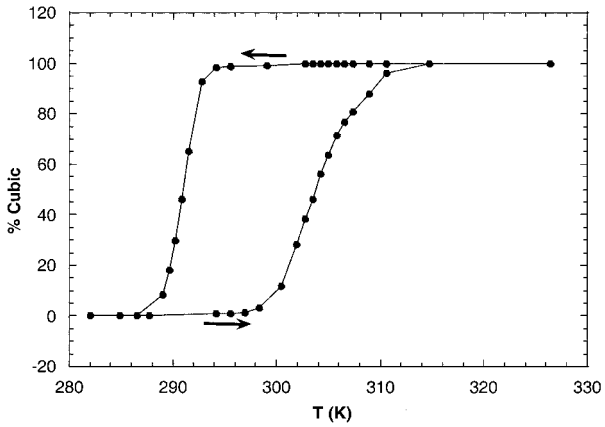

Figure 4. Ratio α of the cubic phase vs temperature through the transition, on heating and cooling. The ratio is determined from a least-squares refinement of the recorded diffraction pattern. Shaded regions correspond to biphasic domains.

An interesting point is the asymmetry observed on heating and on cooling. The transition is more abrupt on cooling, with a smaller biphasic domain than that on heating, which can be explained by a phenomenon similar to supercooling. We can relate this to the difference observed in the specific heat measurements (Figure 1). On cooling, the peak of C_p/T is smaller than the peak on heating. In the same sense, the gain in

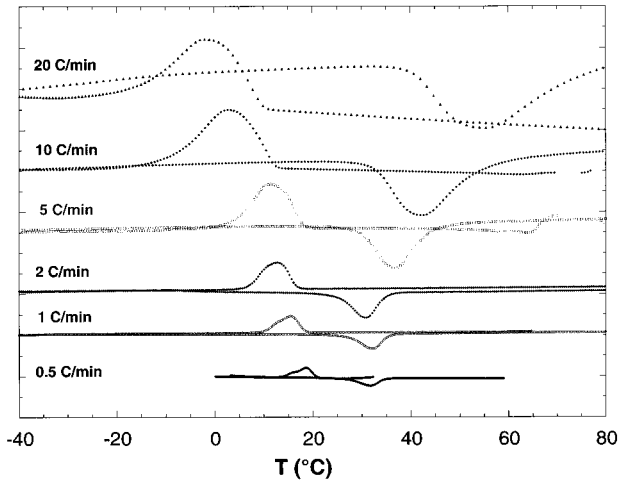

Figure 5. Differential scanning calorimetry (DSC) of $LiMn_2O_4$ between 233 and 353 K, with heating and cooling rates varying from 0.5 to 20 K/min.

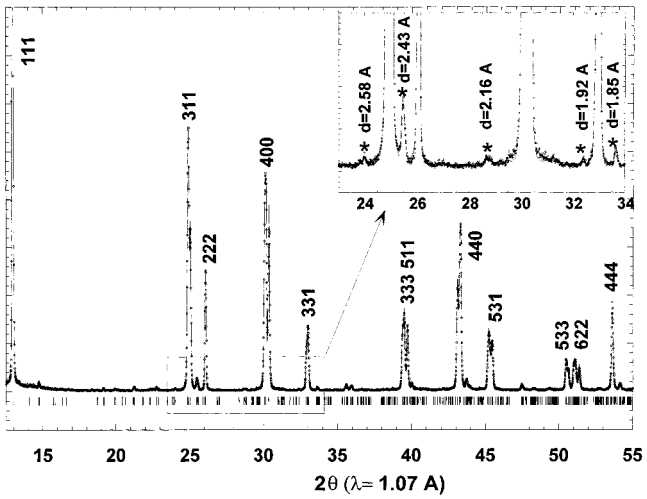

Figure 6. Observed and calculated X-ray diffraction patterns (λ = 1.07 Å) of the orthorhombic form of $LiMn_2O_4$ at 100 K. The insert is a zoom showing some superlattice reflections (marked by a star).

entropy is much higher on heating (17.8 J/K/mol), than that on cooling (14.2 J/K/mol).

III. Refinement of the Structure at 100 K (Synchrotron X-Ray). A recent paper reports the indexing of a neutron diffraction pattern of $LiMn_2O_4$ at 100 K in a tetragonal cell with $a = b = 17.5402(5)$ Å and $c = 8.205\ 15(28)$ Å in the $I4_1/amd$ space group.[17] This cell is deduced from ours by a 45° rotation of [100] and [010], so that the total cell volume is divided by 2 at the same time as the number of formula per unit. We wished to further investigate the existence, or not, of tetragonal symmetry in the low-temperature form of $LiMn_2O_4$.

The X-ray pattern (reflection geometry, aluminum plate) of the low-temperature phase of $LiMn_2O_4$ at 100 K is plotted in Figure 6. The superstructure reflections, due to the charge ordering, are clearly observed, whereas they were very barely visible in transmission mode using a capillary (Figure 2). For example, the most intense superlattice reflections ((2 10 0) and (10 2 0)) at $d = 2.43$ Å can be clearly seen in Figure 6. At 100 K,

(17) Wills, A. S.; Raju, N. P.; Greedan, J. E. *Chem. Mater.* **1999**, *11* (6), 1510.

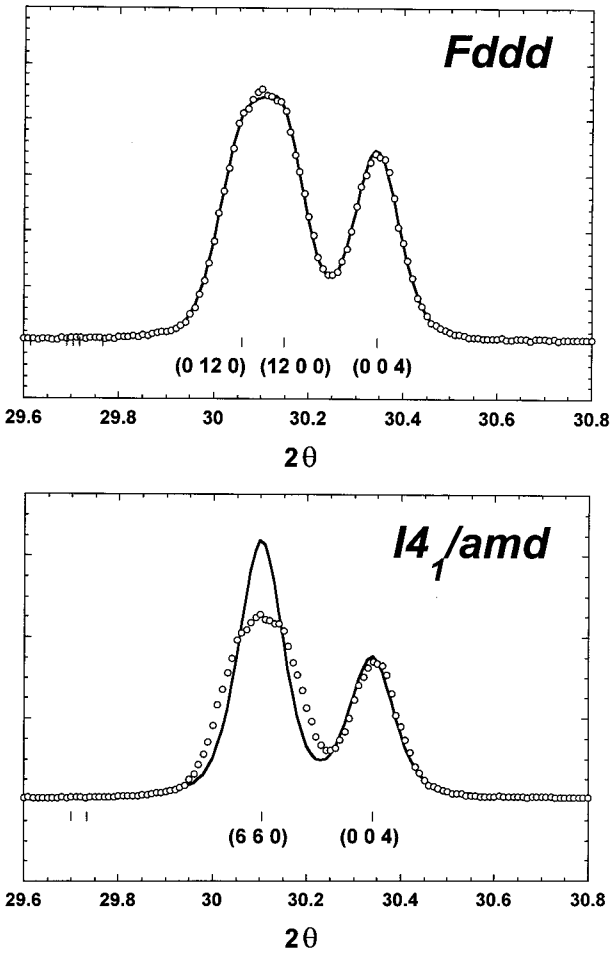

Figure 7. Profile matching of the X-ray diffraction patterns (λ = 1.07 Å) of $LiMn_2O_4$ at 100 K, using the tetragonal cell[17] with space group $I4_1/amd$ and lattice parameters $a = 17.5189(1)$, $b = 17.5189(1)$, and $c = 8.1956(1)$ Å, compared to the profile matching of our orthorhombic cell with space group *Fddd*.

the structure is still orthorhombic, and the superlattice reflections due to the charge ordering are intense. We used the atomic positions refined from the neutron data at 230 K to refine the X-ray pattern. Only the lattice parameters, the overall temperature factor, and the profile parameters were allowed to vary. The refinement was good, with lattice parameters $a = 24.741(1)$, $b = 24.816(1)$, and $c = 8.196(1)$ Å. The total number of reflections is 1138. The conventional Rietveld R factors are: $R_P = 7.94\%$, $R_{WP} = 11.7\%$, $R_{exp} = 7.40\%$, and $\chi^2 = 2.51$. If we refine the Li, Mn, and O atomic positions, the refinement is stable but does not lead to any significant improvement. We preferred to keep them constant as the atomic positions determined from neutron are more reliable, especially for lithium and oxygen. Table 2 contains the observed and calculated intensities for each (hkl) reflection. The reflections marked with a star correspond to the peaks resulting from the orthorhombic distortion of the cubic cell. The indices of their corresponding (hkl) values are indicated. All the others are superlattice reflections induced by the tripling of the cell along a and b. Note that the most intense superlattice reflections are located at $d = 4.18$, 2.43, 1.75, 1.57, 1.44, and 1.33 Å.

Note that the tetragonal cell proposed by Wills et al.[17] in the space group $I4_1/amd$ cannot index our pattern by profile refinement, as demonstrated in Figure 7.

Table 2. Intensities (observed and calculated) of the (*hkl*) Reflections of the Synchrotron X-ray Diffraction Diagram at 100 K[a]

hklc	*h*	*k*	*l*	*D*(*A*)	I_{obs}	I_{calcd}	io−ic	*hklc*	*h*	*k*	*l*	*D*(*A*)	I_{obs}	I_{calcd}	io−ic
111*	3	3	1	4.7562	2268.7	2279.8	−11.2	*	3	15	1	1.5912	154.3	161.2	−6.9
	4	4	0	4.3802	7.6	3.0	4.6	511*	15	3	1	1.5870	171.8	173.4	−1.6
	1	5	1	4.1842	11.0	12.4	−1.4	333*	9	9	3	1.5854	53.5	51.7	1.8
	5	1	1	4.1756	2.9	3.7	−0.7	*	3	3	5	1.5781	183.6	174.2	9.4
	2	0	2	3.8899	1.6	2.0	−0.4		2	10	4	1.5672	9.9	10.7	−0.8
	1	7	1	3.2260	2.8	3.6	−0.8		10	2	4	1.5654	4.5	5.2	−0.7
	7	1	1	3.2181	2.2	2.7	−0.5		11	7	3	1.5594	2.3	3.9	−1.7
	0	8	0	3.1020	2.8	2.4	0.4		1	5	5	1.5534	1.3	2.0	−0.8
*	6	6	0	2.9202	2.3	2.6	−0.4		5	13	3	1.4919	2.3	2.2	0.2
220*	0	6	2	2.9110	3.9	3.3	0.6	*	12	12	0	1.4601	304.0	303.7	0.3
*	6	0	2	2.9067	4.7	3.7	1.0	440*	0	12	4	1.4555	305.1	305.5	−0.4
	8	4	0	2.7678	2.5	3.0	−0.5	*	12	0	4	1.4533	314.1	316.6	−2.4
	5	7	1	2.7187	4.5	2.8	1.7		10	14	0	1.4409	14.1	12.3	1.8
	1	3	3	2.5799	3.0	2.7	0.2		14	10	0	1.4395	15.1	13.1	1.9
*	3	9	1	2.4913	397.6	399.3	−1.7		1	17	1	1.4347	5.4	4.9	0.5
311*	9	3	1	2.4859	391.6	388.1	3.5		17	1	1	1.4306	2.3	2.5	−0.2
*	3	3	3	2.4745	384.2	387.1	−2.8	*	9	15	1	1.3968	67.5	68.4	−0.9
	2	10	0	2.4331	23.2	22.9	0.3	*	15	9	1	1.3948	71.9	73.0	−1.1
	10	2	0	2.4264	10.4	10.1	0.3	531*	3	15	3	1.3947	65.5	66.4	−0.9
222*	6	6	2	2.3781	290.1	290.0	0.0	*	15	3	3	1.3919	72.0	69.9	2.1
	1	11	1	2.1667	3.0	4.1	−1.1	*	3	9	5	1.3888	73.5	72.9	0.6
	1	7	3	2.1557	1.5	2.3	−0.8	*	9	3	5	1.3879	70.1	69.7	0.4
*	0	12	0	2.0680	456.7	458.4	−1.7		2	14	4	1.3327	11.1	10.5	0.6
400*	12	0	0	2.0618	480.6	474.8	5.8		14	2	4	1.3305	2.2	2.0	0.2
*	0	0	4	2.0489	471.7	473.1	−1.4	*	9	15	3	1.2582	49.5	49.1	0.4
*	9	9	1	1.8941	92.0	90.4	1.6	533*	15	9	3	1.2568	51.3	50.3	1.0
331*	3	9	3	1.8891	94.4	94.6	−0.2	*	9	9	5	1.2539	48.8	48.4	0.4
*	9	3	3	1.8867	91.9	93.1	−1.2	*	6	18	2	1.2456	73.8	73.7	0.2
	1	13	1	1.8539	5.0	4.9	0.1	622*	18	6	2	1.2429	74.0	73.7	0.3
	11	7	1	1.8502	4.4	4.6	−0.1		1	13	5	1.2420	2.9	2.8	0.0
	4	6	4	1.7601	2.9	3.3	−0.4	*	6	6	6	1.2373	72.9	75.5	−2.7
	2	14	0	1.7546	14.0	13.6	0.5		13	5	5	1.2048	1.3	2.8	−1.5
	14	2	0	1.7496	2.9	2.8	0.1	444*	12	12	4	1.1891	246.9	240.9	6.0
	5	13	1	1.7404	6.6	6.2	0.4		10	14	4	1.1786	8.2	10.3	−2.1
	13	5	1	1.7367	6.3	6.8	−0.5		14	10	4	1.1779	8.6	10.7	−2.1
	1	11	3	1.7352	2.4	2.6	−0.2								

[a] Reflections are indexed in the $a = 24.7414(4)$, $b = 24.8157(4)$, and $c = 8.1956(2)$ Å supercell, space group *Fddd*. Only reflections with $I/I_{max} > 0.1\%$ are indicated.

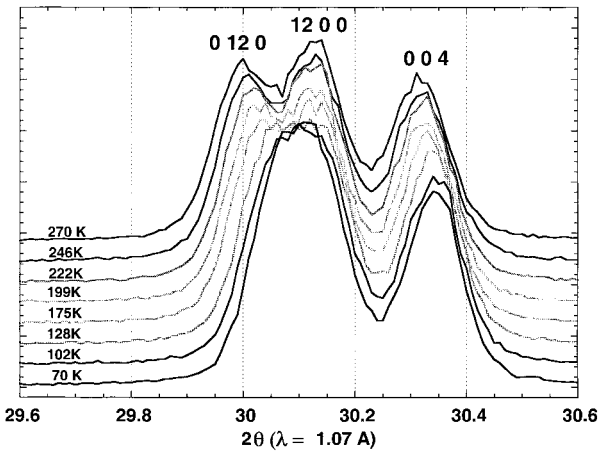

Figure 8. Evolution of the orthorhombic peaks from 270 to 70 K, with the synchrotron radiation ($\lambda = 1.07$ Å).

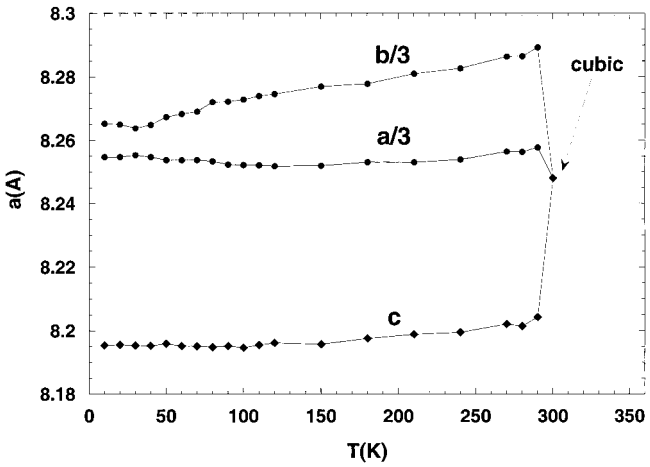

Figure 9. Evolution of the lattice parameters of the orthorhombic phase, determined via X-ray diffraction ($\lambda = 1.5418$ Å).

IV. Evolution of the Orthorhombic Phase at Low Temperature. The evolution of the orthorhombic distortion with temperature down to 70 K was followed using Synchrotron X-ray radiation (Figure 8). There is clearly an anisotropic evolution of the three lattice parameters: the (12 0 0) and the (0 12 0) peaks shift toward each other, whereas the (004) peak is only shifted by the thermal expansion.

To confirm this tendency, we performed similar measurements on a conventional X-ray diffractometer ($\lambda = 1.5418$ Å) at temperatures varying from 300 to 13 K. Figure 9 presents the evolution of the cell parameters determined by cell-constrained profile refinement. The data show an anisotropic variation of the three parameters versus temperature as the cell parameters *a* and *b* become closer on cooling.[18] However, our samples

(18) Tabuchi, J.; Numata, T.; Shimakawa, Y.; Shirakata, M. *Mater. Res. Soc. Symp. Proc.* **1998**, *496*, 287.

never become tetragonal when cooled below 60 K, contrary to other reports.[10,17] At 70 K, the apparent two peaks can be easily decomposed into three peaks in the same way as those in Figure 7 (data recorded at 100 K) if we take into account the resolution of the instrument. Figure 9 indicates a clear orthorhombicity of the spinel at this temperature. A careful observation of the X-ray diagrams does not show any new phase transformation. This tends to contradict our previous suggestion on the existence of a new totally ordered phase around 100 K.[9] Recent infrared measurements on powdered $LiMn_2O_4$ also exclude the onset of a new structural phase transition between 290 and 10 K.[7]

We notice, additionally, that antiferromagnetic reflections appear in the neutron diffraction patterns below 60 K. The propagation vector between the nuclear and the magnetic structure is incommensurate. The study of the magnetic structure is under way and will be detailed in a later paper. Notice that at 1.5 K the nuclear structure is the same as that at 230 K: it is still orthorhombic.

Conclusion

We carefully studied and characterized the room-temperature transition of $LiMn_2O_4$ using X-ray diffraction techniques. We have shown that it is a first-order transition with the occurrence of a biphasic domain. The volume remains constant up to first order during the transition. X-ray diffraction and specific heat measurements indicate that it is more difficult (lower entropy) to form the orthorhombic ordered phase on cooling than to form the cubic disordered phase (higher entropy) on heating. The structure remains orthorhombic in the whole range of temperatures studied, down to 1.5 K, with an anisotropic variation of the lattice parameters. X-ray diffraction tends to exclude the onset of a transition to tetragonal symmetry at low temperatures.

Acknowledgment. We thank Pr. Ryoji Kanno for having performed the X-ray (Cu Kα) diffraction versus temperature experiment. G.R. thanks Union-Minière and ANRT for a “CIFRE” financial support.

CM9910963